



### AN EXPLORATORY DATA ANALYSIS OF ELECTROENCEPHALOGRAMS USING THE FUNCTIONAL BOXPLOTS APPROACH

Duy Ngo, Hernando Ombao, Ying Sun, Marc G. Genton, Jennifer Wu, Ramesh Srinivasan and Steven Cramer

Journal Name:	Frontiers in Neuroscience
ISSN:	1662-453X
Article type:	Original Research Article
First received on:	13 May 2015
Revised on:	12 Jul 2015
Frontiers website link:	<a href="http://www.frontiersin.org">www.frontiersin.org</a>

<sup>1</sup> An Exploratory Data Analysis of Electroencephalograms Using the  
<sup>2</sup> Functional Boxplots Approach

<sup>3</sup> Duy Ngo <sup>\*</sup>, Ying Sun <sup>†</sup>, Marc G. Genton <sup>†</sup>, Jennifer Wu <sup>‡</sup>,  
Ramesh Srinivasan <sup>§</sup>, Steven C. Cramer <sup>‡</sup>, Hernando Ombao<sup>1</sup> \*

<sup>4</sup> July 11, 2015

<sup>5</sup> **Abstract**

<sup>6</sup> Many model-based methods have been developed over the last several decades for analysis of elec-  
<sup>7</sup> troencephalograms (EEG) in order to understand electrical neural data. In this work, we propose to  
<sup>8</sup> use the functional boxplot to analyze log periodograms of EEG time series data in the spectral domain.  
<sup>9</sup> The functional boxplot approach produces a median curve – which is not equivalent to connecting  
<sup>10</sup> medians obtained from frequency-specific boxplots. In addition, this approach identifies a functional  
<sup>11</sup> median, summarizes variability and detects potential outliers. By extending functional boxplots anal-  
<sup>12</sup> ysis from one-dimensional curves to surfaces, surface boxplots are also used to explore the variation of  
<sup>13</sup> the spectral power for the alpha (8 – 12 Hertz) and beta (16 – 32 Hertz) frequency bands across the  
<sup>14</sup> brain cortical surface. By using rank-based nonparametric tests, we also investigate the stationarity of  
<sup>15</sup> EEG traces across an exam acquired during resting-state by comparing the spectrum during the early  
<sup>16</sup> vs. late phases of a single resting-state EEG exam.

<sup>17</sup> **Keywords:** EEGs time series, Functional boxplots, Surface boxplots, Spectral Analysis, Band depth,  
<sup>18</sup> Exploratory analysis, Stationarity.

<sup>19</sup> **1 Introduction**

<sup>20</sup> Electroencephalograms (EEGs) have been used for many decades to study the complex spatio-temporal  
<sup>21</sup> dynamics of brain processes (Nunez and Srinivasan [2006]). Due to its excellent temporal resolution  
<sup>22</sup> (sampling rates usually range from 100 – 1000 Hz), EEGs can capture transient changes in brain ac-  
<sup>23</sup> tivity, identify oscillatory behavior and study cross-dependence between EEG components. Since EEGs  
<sup>24</sup> indirectly measure neuronal electrical activity, they can be used to infer the statistical properties of the  
<sup>25</sup> underlying brain stochastic process. One such statistical property is the spectrum (or power spectrum)

---

<sup>\*</sup>Department of Statistics, University of California, Irvine, USA

<sup>†</sup>CEMSE Division, King Abdullah University of Science and Technology

<sup>‡</sup>Department of Anatomy & Neurobiology, University of California, Irvine

<sup>§</sup>Department of Cognitive Sciences, University of California, Irvine

<sup>1</sup>Corresponding author.

which decomposes the total variability in the EEG according to the contribution of oscillations at different frequencies. Most approaches to analyzing EEGs focus immediately on statistical modeling and spectral estimation. Here, we offer a systematic framework for exploring structures, patterns and features in the signal – prior to formal modeling. We explore the spectral properties only in a single channel using EEG traces from several epochs.

One approach to estimating the spectrum using EEG traces is to fit a parametric time domain model, such as the autoregressive moving average (ARMA) model. Applications of parametric modeling of EEGs have a long history. See Bohlin [1973], Isaksson et al. [1981] Jain and Deshpande [2004] and Krystal et al. [1999] among many others. When the spectrum of the EEG evolves over time (e.g., within an epoch), one could still use the ARMA model but allow the coefficients to vary over time. A key element in ARMA models is the order of the autoregressive (AR) and moving average (MA) components. These can be obtained objectively using an information-theoretic criterion such as the Akaike information criterion (AIC) and the Bayesian information criterion (BIC). Using these criteria, we obtain an optimal AR and MA order that jointly gives the best fit with the least complexity (as determined by the orders). BIC puts a heavier penalty for complexity compared to AIC and thus often gives a model with lower orders (lower complexity). From the parametric fit, we derive the estimates of the auto-correlation function and the spectrum. The theoretical background for parametric models are developed in Priestley [1981], Shumway and Stoffer [2000] and Brockwell and Davis [2009]).

One could also estimate the spectrum without resorting to a parametric model. Under this approach, the EEGs are considered to be superpositions of sines and cosines (Fourier waveforms) with different frequencies and random amplitudes. These random amplitudes (or coefficients) are computed using the fast Fourier transform (FFT). The squared magnitude of these amplitudes, often called the periodograms, are the data-analogues of the spectrum defined on discrete frequencies. The theoretical background on the frequency domain approach to time series is developed in Brillinger [1981] and Percival and Walden [1993]. This approach to analyzing EEGs continues to be popular in the cognitive and brain sciences. The following papers cover both methods and applications of spectral analysis to EEGs: Bressler and Freeman [1980], Makeig [1993], Pfurtscheller and Aranibar [1979] and Srinivasan and Deng [2011], to name a few.

The common practice prior to spectral estimation is to pre-process EEGs, often to remove artifacts Makeig et al. [1996]. After artifact rejection and segmentation according to epochs, the spectrum is estimated from each EEG trace. As noted, there is a lack a systematic framework for exploring structures, patterns and features in the signal – prior to formal modeling. Due to the complexity of EEG data, exploratory data analysis (EDA) plays an important role, especially when data are recorded from many epochs or trials during an experiment. For example, it is often expected that brain responses to the same stimulus ought to be relatively uniform, with minimal variation across epochs. In contrast, greater variability across epochs may be expected during neuroimaging studies that examine the brain in resting-state, as cognitive processes can vary within and across sessions for individual subjects and across subjects. An appropriate EDA methods can provide insights into features of EEG, including similarities and variability of the brain responses across epochs to facilitate the statistical model. In this paper, we propose to use the functional boxplot (FBP) method originally developed by Sun and Genton [2011] to address these questions.

The methods presented in this paper are motivated by a motor skill acquisition study at the Neuro-rehabilitation laboratory at the University of California, Irvine (Principal Investigator: Steven C. Cramer).

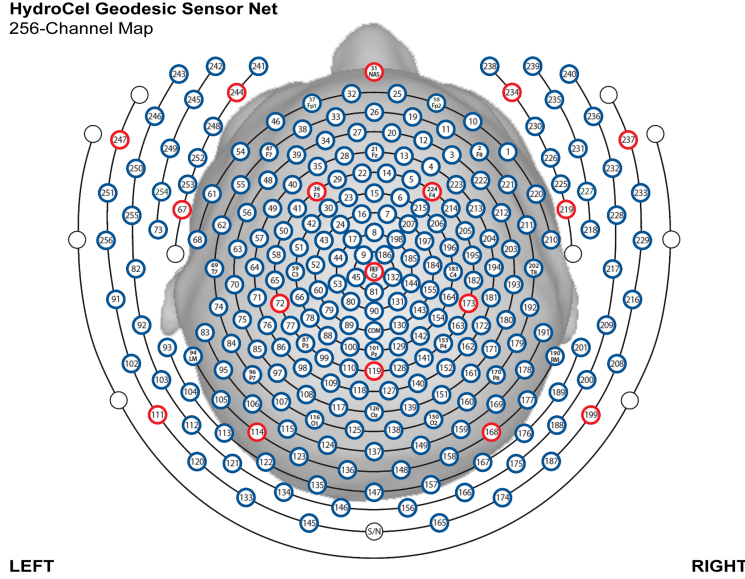


Figure 1: Map of channels on the scalp.

In the previous study, EEG was recorded from 17 subjects both during resting-state prior to motor skill training and during motor skill training using dense-array EEG (256 electrodes) as shown in Figure 1. The resting-state EEG exam was three minutes, and during post-processing, was segmented into one-second non-overlapping epochs. As demonstrated in Wu et al. [2014], the spectral features of the resting-state EEGs when combined with a partial least squares regression analysis, was predictive of an individual's subsequent ability to acquire a novel motor skill. These may be of clinical importance to the field of rehabilitation, as improved methods for stratifying patients may significantly improve response to treatment and assist allotment of limited resources.

We present an exploratory spectral analysis (ESA) of resting-state EEG traces using functional boxplots for one subject. In spectral analysis, the spectrum is an important stochastic property of the signal. It indicates the amount (or proportion) of variance that is explained by each frequency bin. Thus the spectrum or the log spectrum of the EEG signal can be used to examine relative amounts of variability explained by slow (delta or theta) waves and fast (alpha or beta) waves. Throughout this analysis, we obtain a *sample* spectral curve by smoothing the log periodograms of each one-second EEG epoch, and treat it as one observation unit in the FBP. By using the FBP, we address three primary objectives. The *first* objective is to identify the median, i.e., the most characteristic spectral curve rather than the pointwise frequency-specific medians. In addition, outliers are demonstrated by their unusual sample log spectral curve, and can be caused by extra-brain artifacts, including eye blinks, eye movements and muscle movements in the EEG signal. Subsequently, confirmed outliers will be removed from subsequent analyses. The advantage of the FBP approach, over the usual pointwise boxplot method, is that it identifies epochs that have potential outlying spectral curves.

The *second* objective is to compare the median curves and the variability of the spectral curves from multiple phases of the resting state period. To test the stationarity of the EEG signal over the entire recording, we compare the spectral curves and the frequency-specific spatial distribution of spectral power

92 during the early phase (first 60 epochs) versus the late phase (last 60 epochs). Evidence against stationarity must be taken seriously since this would suggest an evolution of brain processes across the recording  
 93 (Fiecas and Ombao [2015]). Moreover, the FBP approach is able to provide some characterization of  
 94 the variation of the sample log spectral curves across EEG recording. In experiments comparing more  
 95 than one group (e.g., healthy controls vs patients with stroke), it would be also interesting to determine  
 96 whether groups differ with respect to consistency (uniformity) of the EEG signal over time.  
 97

98 The *third* objective is to investigate the spatial variability of spectral power across the brain for a  
 99 given frequency band using the surface boxplot, which is a generalization of the FBP. Using the surface  
 100 boxplots approach, it is possible to identify cortical regions (or channels) that, relative to the other  
 101 channels, exhibit a high proportion of beta power. The beta band is particular interest to neuroscientists,  
 102 as changes in beta activity have a good association with motor function (Roopun et al. [2006] and Joundi  
 103 et al. [2012]).

104 The remainder of the paper is organized as follows. In Section 2, we present a comprehensive ex-  
 105 ploratory method which consists of the following: a review of the spectra in Section 2.1, a demonstra-  
 106 tion of automatic bandwidth selector for periodogram smoothing using the gamma generalized crossvalidation  
 107 criterion in Section 2.2, some remarks on smoothing the periodogram in Section 2.3, a description of the  
 108 functional boxplots in Section 2.4, a description of the surface boxplots in Section 2.5, and a demonstra-  
 109 tion of testing for differences in mean curves between families of curves in Section 2.6. In Section 3, we  
 110 examine the finite sample performance of the proposed exploratory method. In Section 4, the resting-state  
 111 EEG data are analyzed. Finally, in Section 5, conclusions and future work are discussed.

## 112 2 Method for Exploratory Spectral Analysis (ESA)

113 In this section, we review the methods that are needed for ESA of the EEG data. In Section 2.1, we first  
 114 formally define the spectrum and then discuss a consistent estimator which is obtained by smoothing the  
 115 periodogram using a bandwidth that is automatically selected by the gamma generalized cross-validation  
 116 (Gamma-GCV) method described in Section 2.2. Next, we highlight two remarks on smoothing the  
 117 periodogram in Section 2.3, then we present the functional boxplots method in Section 2.4 and surface  
 118 boxplots method in Section 2.5. Finally, we present a rank sum test which tests for differences in median  
 119 curves or surfaces between families of curves or surfaces in Section 2.6.

### 120 2.1 Spectrum

121 The spectrum of an EEG signal (which is assumed to be stationary) can give the amount of variance  
 122 contributed by oscillatory components (from delta to beta band activity). Let  $X(t)$ ,  $t = \dots, -1, 0, 1, \dots$  be  
 123 a zero-mean stationary time series with covariance function  $\gamma(\tau) = E(X(t)X(t + \tau))$  ( $\tau = \dots, -1, 0, 1, \dots$ )  
 124 that is assumed to be absolutely summable, i.e.,  $\sum_{\tau=-\infty}^{\infty} |\gamma(\tau)| < \infty$ . The spectrum, denoted  $f(\omega)$ , is  
 125 defined to be

$$f(\omega) = \sum_{\tau=-\infty}^{\infty} \gamma(\tau) e^{-i2\pi\omega\tau}, \quad \omega \in \left[-\frac{1}{2}, \frac{1}{2}\right].$$

126 The starting point for estimating  $f(\omega)$  is the periodogram. Denote  $I(\omega_k)$  to be the periodogram computed  
 127 from a finite sample of the stationary process  $X(0), X(1), \dots, X(T - 1)$  at frequency  $\omega_k = k/T$  which is

128 defined to be

$$I(\omega_k) = \frac{1}{T} \left| \sum_{t=0}^{T-1} X(t) e^{-i2\pi\omega_k t} \right|^2, \quad k = -[\lceil T/2 \rceil] - 1, \dots, [\lceil T/2 \rceil],$$

where  $[\lceil T/2 \rceil]$  is the quotient of  $T/2$ . To characterize the spectra of the EEG signals, we classify the

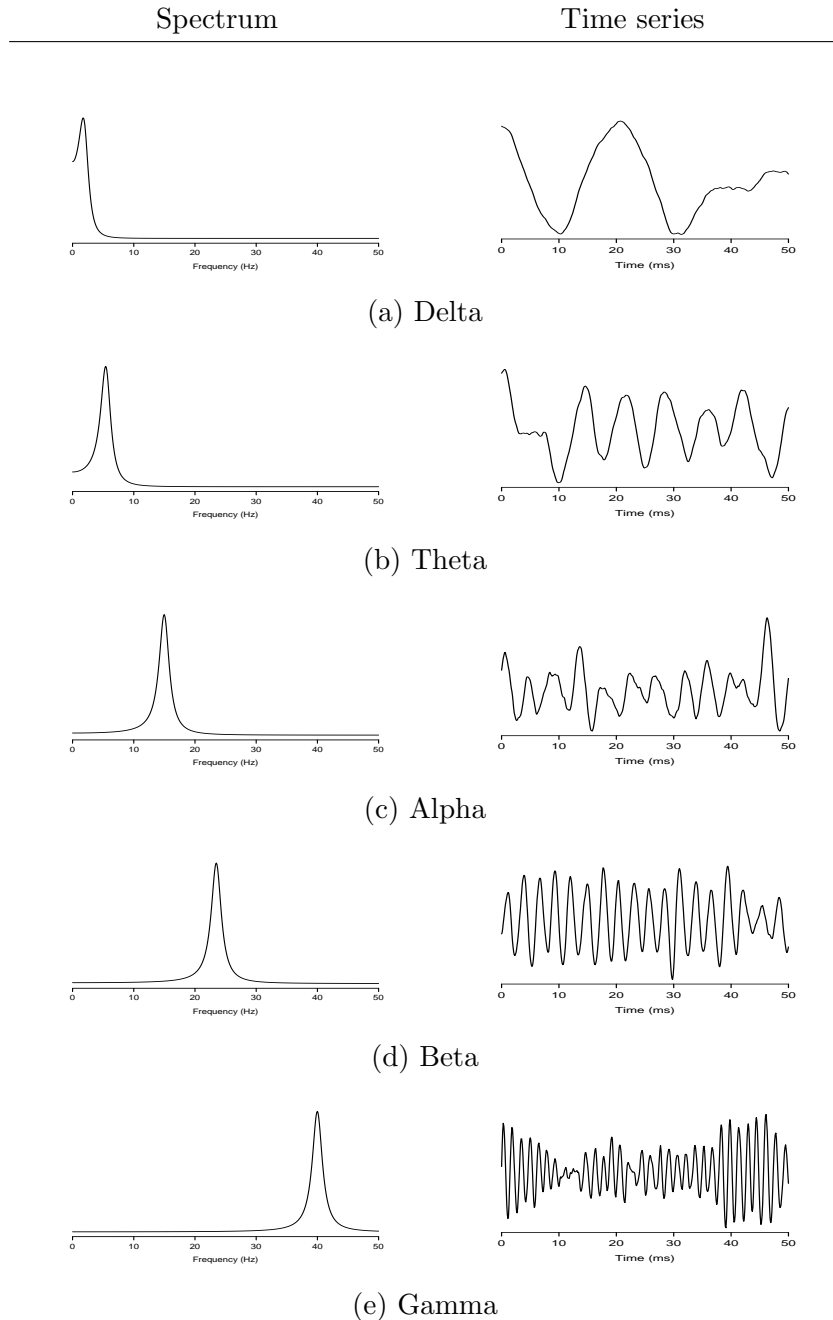


Figure 2: Left: the spectrum of second order auto-regressive processes AR(2) with power concentrated at the delta (0-4 Hertz), theta (4-8 Hertz), alpha (8-16 Hertz), beta (16-32 Hertz) and gamma (32-50 Hertz) bands. Right: realizations from each corresponding AR(2) process.

129

130 oscillatory patterns of periodograms into four primary frequency bands: delta (0-4 Hz), theta (4-8 Hz),

131 alpha (8-16 Hz), beta (16-32 Hz) and gamma (32-50 Hz) as shown in Figure 2. Since each frequency band  
 132 is defined by a range, we define  $\widehat{S}(\Omega)$  to be the estimated spectral power at the  $\Omega$  band:

$$\widehat{S}(\Omega) = \int_{\omega \in \Omega} I(\omega) d\omega.$$

133 It is well known that the periodogram  $I(\omega_k)$  is an asymptotically unbiased estimator for  $f(\omega_k)$ , but it  
 134 is inconsistent because its variance approaches a positive constant when  $T \rightarrow \infty$ . Therefore, to reduce  
 135 the variance, we smoothed the periodogram. A number of nonparametric smoothing methods have been  
 136 proposed including the kernel smoother (Lee [1997], Ombao et al. [2001]), wavelet (Gao [1997]), smoothing  
 137 spline (Wahba [1980], Pawitan and O'sullivan [1994]), or local polynomial (Fan and Kreutzberger [1998]).  
 138 For kernel smoothing, (Ombao et al. [2001]) developed an automatic span selector via the generalized  
 139 crossvalidation criterion for generalized additive models based on the *deviance* which is discussed in  
 140 Section 2.2.

## 141 2.2 Automatic Span Selector Using the Gamma Generalized Crossvalidation Method

142 From Brillinger [1981] (Theorem 5.2.6),  $I(\omega_k)$  follows an asymptotic distribution

$$I(\omega_k) \sim \begin{cases} \text{Gamma}(1, f(\omega_k)) & k = 1, \dots, T/2 - 1 \\ \text{Gamma}(\frac{1}{2}, 2f(\omega_k)) & k = 0, T/2, \end{cases}$$

143 where  $I(\omega_0), \dots, I(\omega_{T/2})$  are independent. As a caveat, we note here that the actual result requires that  
 144 the number of frequencies is fixed and does not depend on  $T$ . However, in most applications, this is often  
 145 ignored. This result can be equivalently stated as  $I(\omega_k)/f(\omega_k) \sim \epsilon_k$  where  $\epsilon_k \stackrel{\text{d}}{\sim} \chi^2(1)$  when  $k = 0$  or  
 146  $T/2$  and  $\epsilon_k \stackrel{\text{d}}{\sim} \frac{1}{2}\chi^2(2)$  when  $k = 1, \dots, T/2 - 1$ . As noted, we need to smooth the periodogram  $I(\omega_k)$   
 147 to produce a consistent estimator for  $f(\omega_k)$ . Let  $\widehat{f}_p(\omega_k)$  be a smoothed periodogram estimator of  $f(\omega_k)$   
 148 which we define to be

$$\widehat{f}_p(\omega_k) = \sum_{j=-p}^p W_{p,j} I(\omega_{k+j}) \quad k = 0, \dots, T/2, \text{ and } j = -p, \dots, p$$

149 where  $2p+1$  is the smoothing span and  $W_{p,j}$  are nonnegative weights that satisfy the following conditions  
 150 for any fixed  $p$ :

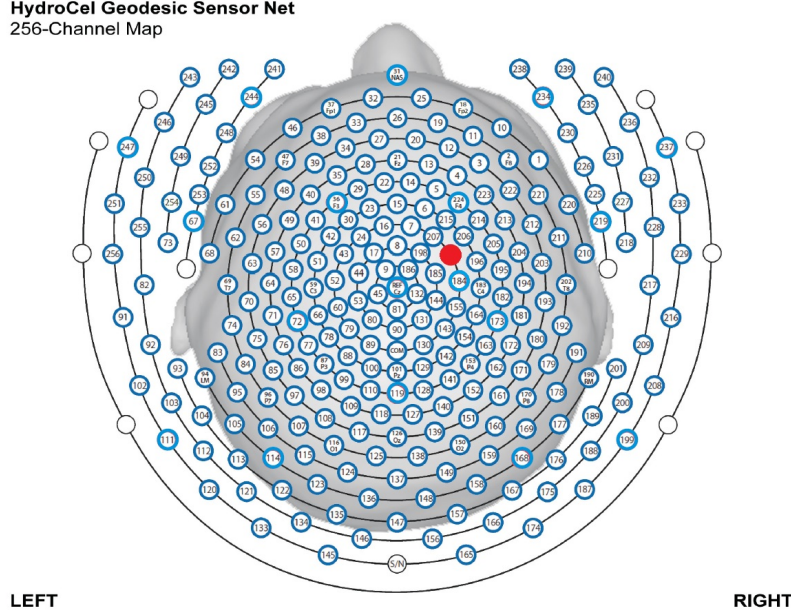
$$W_{p,j} = W_{p,-j} (j = 1, \dots, p), \quad \sum_{j=-p}^p W_{p,j} = 1.$$

151 Generally, the weights are chosen so that  $W_{p,j}$  is a decreasing function of  $p$ , but Priestley [1981] shows that  
 152 the choice of the weights  $W_{p,j}$  is of secondary importance to the value of the span or bandwidth. Thus, for  
 153 simplicity, we use the boxcar smoother with weights defined by  $W_{p,j} = 1/(2p+1)$  for all  $j = -p, \dots, p$ . The  
 154 gamma generalized crossvalidation method selects  $p$  to minimize the generalized crossvalidated deviance  
 155 function

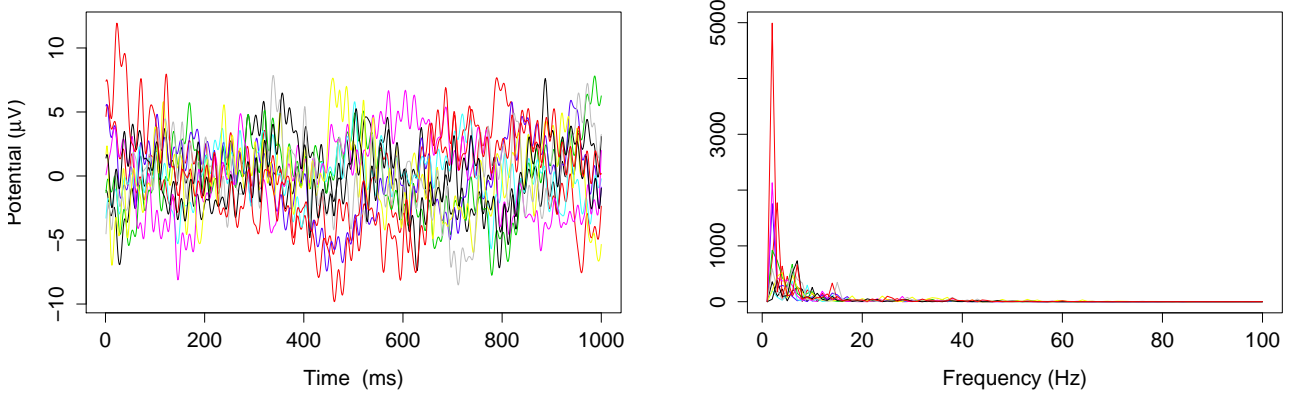
$$GCV(p) = \frac{M^{-1} \sum_{j=0}^{M-1} D(I(\omega_j), \widehat{f}_p(\omega_j))}{(1 - \text{tr}(H_p)/M)^2},$$

156 where  $M = T/2 + 1$ . The deviance  $D(I(\omega_j), \hat{f}_p(\omega_j))$  can be chosen as  $q_j\{-\log(I(\omega_j)/\hat{f}_p(\omega_j)) + (I(\omega_j) - \hat{f}_p(\omega_j))/\hat{f}_p(\omega_j)\}$  (McCullagh and Nelder [1989]). Here,  $q_j = 1 - 0.5\mathcal{I}\{j = 0, M - 1\}$ , and  $\mathcal{I}$  is the indicator function. The  $H_p$  is the smoother matrix with smoothing parameter  $p$ , and the term  $(1 - \text{tr}(H_p)/M)^2$  often referred to as the model degrees of freedom, can be expressed in terms of the weight at the center of the smoothing window:  $(1 - W_{p,0})^2$ . Then, the generalized crossvalidated deviance function can be written as

$$GCV(p) = M^{-1} \sum_{j=0}^{M-1} q_j \left\{ \frac{-\log(I(\omega_j)/\hat{f}_p(\omega_j)) + (I(\omega_j) - \hat{f}_p(\omega_j))/\hat{f}_p(\omega_j)}{(1 - W_{p,0})^2} \right\}.$$



(a) Red circle represents right pre-motor region (channel 197) on the scalp



(b) EEG time series of right pre-motor region (channel 197) (c) Raw periodograms after filtering out frequency 60 HZ by averaging method

Figure 3: EEG time series and raw periodograms after filtering out frequency 60 HZ by averaging method of channel 197 (right pre-motor region) for the first 10 traces.

163 2.3 Remarks

For frequencies over 100 Hz, the periodogram values are almost negligible because the signals underwent low-pass filtering at 100 Hz. , so for simplicity, we will only show the spectrum over the frequency range of 0 – 100 Hertz. In Figure 3, we show the location of channel 197 in right pre-motor region at the resting-state. Figure 4 gives an illustration of smoothing the periodograms for randomly selected epochs 3, 85 and 160 for a fixed channel 197. It can be seen that the power at these periodograms are dominated by low frequencies, and the values of smoothing span minimizing the generalized crossvalidated deviance function are about 3-5. Also, the smoothing lines reasonably approximate the periodograms and the small bandwidths preserve the peaks. Second, since the distribution of  $I(\omega_k)$  is a multiple of the spectral

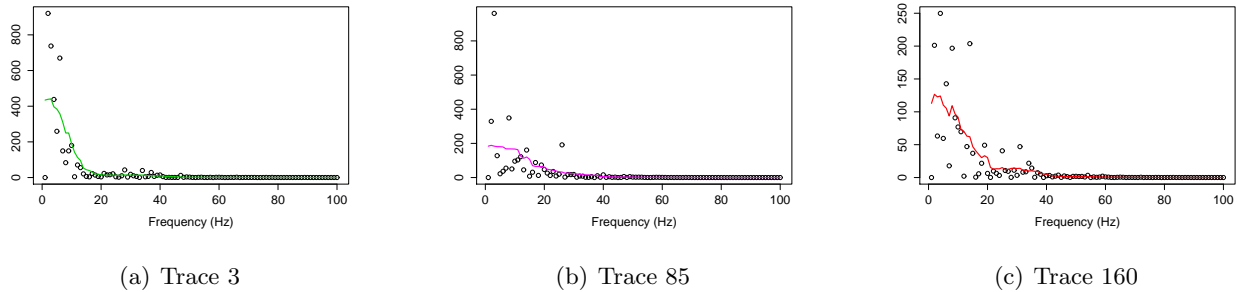


Figure 4: Smoothing periodograms at randomly selected epochs 3, 85 and 160 of channel 197 (in the right pre-motor region) using the bandwidth that was automatically selected by the gamma generalized crossvalidation (gamma-GCV) method.

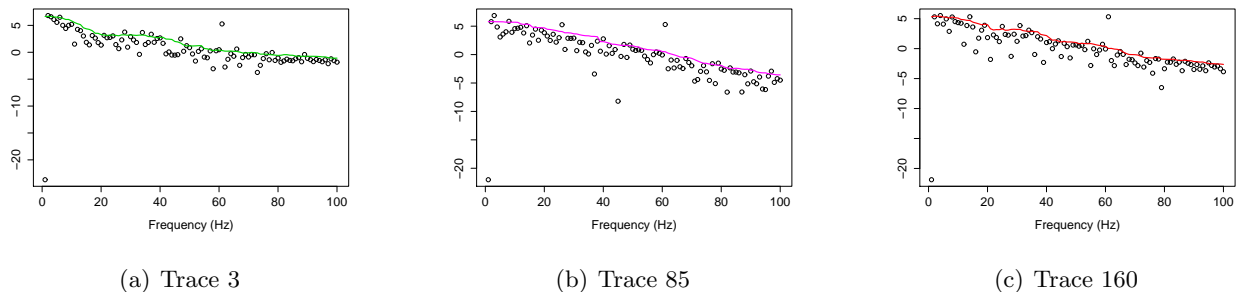


Figure 5: Log bias-corrected periodograms of epochs 3, 85 and 160 from Channel 197 (Right pre-motor region)

density, its variance (which depends on  $f(\omega_k)$ ) also changes across the frequencies  $\omega_k$ . To stabilize the variance across frequencies and to standardize comparisons of median curves across two phases (early vs late phases of the resting-state EEG recording) we will use the log transformed periodograms. It is convenient then, that the variance of the log periodograms at each frequency is constant and takes the approximate value of  $\frac{\pi^2}{6}$ . Moreover, while the periodogram is approximately unbiased for the spectrum, the log periodogram is no longer (approximately) unbiased for the log spectrum due to Jensen's inequality. This is easily fixed by adding the Euler Mascheroni constant 0.57721 to log transformed periodograms

179 to obtain the log bias-corrected periodograms (Wahba [1980]). Let  $g(\omega_k)$  be the true log spectrum, then  
 180  $Y_r(\omega_k)$ , the log bias of the corrected periodogram at epoch  $r$ , is defined as

$$Y_r(\omega_k) = g(\omega_k) + 0.57721, \quad k = 0, 1, \dots, T/2.$$

181 Figure 5 gives the log bias-corrected periodograms,  $Y_r(\omega_k)$ , corresponding to Figure 4. Throughout this  
 182 paper, we will apply the gamma crossvalidation method to obtain the optimal smoother of log bias-  
 183 corrected periodograms.

## 184 2.4 Functional Boxplots

185 The functional boxplot is constructed in a similar manner to the classical (pointwise) boxplot. Each  
 186 observation will be sorted based on decreasing values of some depth measure, and band depth is one notion.  
 187 A curve is said to be “deeply situated” within a sample of curves if it is covered by many bands from pairs  
 188 of curves. This idea is an extension of a pointwise boxplot where the median is also located “deep” in a  
 189 sample because it is situated in the middle of the boxplot and hence covered by many pairs of points. Here,  
 190 our observation units are curves (or real-valued functions) which are the log bias-corrected periodograms  
 191  $Y_r(\omega_k)$ ,  $k = 0, \dots, T/2$  over many epochs  $r$ . The notion of a band depth was introduced in López-Pintado  
 192 and Romo [2009] through a graph-based approach to order all sample curves which we briefly describe.  
 193 Suppose that a curve  $Y(\omega_k)$  is the subset of the plane  $G(Y(\omega_k)) = \{(\omega_k, Y(\omega_k)) : \omega_k \in \mathcal{A} = [0, T/2]\}$ .  
 194 The band in  $\mathbb{R}^2$  can be delimited by a number  $J$  of curves, and this number is fixed as  $J = 2$  in our study.  
 195 Now, let  $Y_\alpha, Y_\beta$  be two continuous functions,  $L_k = \min(Y_\alpha(\omega_k), Y_\beta(\omega_k))$ , and  $U_k = \max(Y_\alpha(\omega_k), Y_\beta(\omega_k))$ .  
 196 Then the band delimited by  $Y_\alpha, Y_\beta$  is

$$B(Y_\alpha, Y_\beta) = ((\omega_k, Y'(\omega_k)) : \omega_k \in \mathcal{A}, L_k \leq Y'(\omega_k) \leq U_k).$$

197 Let  $Y_1, \dots, Y_n$  be  $n$  independent sample curves, then the band depth for a given curve  $Y_i$ ,  $i = 1, \dots, n$  is  
 198 defined as

$$BD(Y_i) = \binom{n}{2}^{-1} \sum_{\alpha=1, \dots, n; \beta=1, \dots, n} \mathcal{I}\{G(Y_i) \subseteq B(Y_\alpha, Y_\beta)\}$$

199 where  $\mathcal{I}(\cdot)$  is the indicator function. When  $J = 2$ , there are  $\binom{n}{2}$  possible bands delimited by two curves.  
 200 The limit of the band depth  $BD$  is that it does not measure the proportion of curve inside the band. Thus,  
 201 López-Pintado and Romo [2009] also proposed a modified band depth method (MBD), which measures  
 202 the proportion of a curve  $Y_i$  that is actually in a band:

$$MBD(Y_i) = \binom{n}{2}^{-1} \sum_{\alpha=1, \dots, n; \beta=1, \dots, n} \lambda\{A(Y_i; Y_\alpha, Y_\beta)\}$$

203 where  $A(Y_i; Y_\alpha, Y_\beta) \equiv \{\omega_k \in \mathcal{A} : L_k \leq Y_i \leq U_k\}$ ,  $\lambda(Y_i) = \lambda(A(Y_i; Y_\alpha, Y_\beta))/\lambda(\mathcal{A})$ , and  $\lambda$  is a Lebesgue  
 204 measure on  $\mathcal{A}$ . We notice that the MBD computation will be time-consuming when  $n$  is large, so we use  
 205 an exact fast method from Sun et al. [2012] to compute the MBD for the EEG data.

206 Based on the ranks of the depths of the curves, the functional boxplots can provide the descriptive  
 207 statistics, such as the 50% central region, the median curve, and the maximum and minimum non-  
 208 outlying curves. Moreover, the potential outliers can be detected by the 1.5 times inter-quartile range

(IQR) empirical rule, which is commonly used for classical boxplots. The boundary region is defined as 1.5 times the height of the 50% central region. Any curves outside this region are considered potential outliers. In contrast with a constant factor 1.5 in classical boxplot, a factor 1.5 in functional boxplot can be modified due to potential spatio-temporal outliers. This is because the curves from different locations will be spatially correlated, and there can be dependence in time/frequency for each curve (Sun and Genton [2012a]).

## 2.5 Surface Boxplots

Similar to functional boxplots, one can compute the data depth of all the observations, then order them according to decreasing depth values. Suppose that the observed sample surfaces,  $z_1(s), \dots, z_n(s)$ ,  $s \in \mathcal{S}$ , where  $\mathcal{S}$  is a region in  $\mathbb{R}^2$ . The information unit for such a dataset is the entire surface. To order sample surfaces, we need to generalize univariate order statistics to surfaces. To this end, we generalize the MBD with  $J = 2$  to  $\mathbb{R}^3$  through a volume. Genton et al. [2014] define the sample modified volume depth (MVD) to be

$$MVD_n(z) = \binom{n}{2}^{-1} \sum_{1 \leq i_1 \leq i_2 \leq n} \lambda_r A(z; z_{i_1}, z_{i_2}),$$

where  $A(z; z_{i_1}, z_{i_2}) \equiv \mathbf{s} \in \mathcal{S} : \min_{r=i_1, i_2} z_r(\mathbf{s}) \leq z(\mathbf{s}) \leq \max_{r=i_1, i_2} z_r(\mathbf{s})$  and  $\lambda_r(z) = \frac{\lambda(A(z; z_{i_1}, z_{i_2}))}{\lambda(\mathcal{S})}$ , if  $\lambda$  is the Lebesgue measure on  $\mathbb{R}^3$ . A sample median surface is a surface from the sample with the largest sample modified volume depth value, designed by  $\arg \max_{z \in z_1, \dots, z_n} MVD_n(z)$ . If there are ties, the median will be the average of the surfaces maximizing the sample modified volume depth.

The first step for constructing surface boxplots is the surface ordering. Sample surfaces are ordered from the center outwards based on their MVD values, inducing the order  $z_{[1]}, z_{[2]}, \dots, z_{[n]}$ . The sample  $\alpha$  central region is naturally defined as the volume delimited by the  $\alpha$  proportion ( $0 < \alpha < 1$ ) of the deepest surfaces. In particular, the sample 50% central region is

$$C_{0.5} = \{(\mathbf{s}, z(\mathbf{s})) : \min_{r=1, \dots, [n/2]} z_{[r]}(s) \leq z(\mathbf{s}) \leq \max_{r=1, \dots, [n/2]} z_{[r]}(s)\},$$

where  $[n/2]$  is the smallest integer not less than  $n/2$ . The border of the 50% central region is defined as the inner envelope representing the box in a surface boxplot. This is the surface analogue of the first and third quartiles of the classical boxplot. The median surface in the box is the one with the largest depth value. Because the ordering is from the center outwards, the volume of the central region increases as  $\alpha$  increases. Hence, the maximum envelope, or the outer envelope, is defined as the border of the maximum non-outlying central region. To determine this region, we propose to identify outlying surfaces by an empirical rule similar to the 1.5 times the 50% central region rule in a functional boxplot. The fences (or the upper and lower surface boundaries for flagging potential outliers) are obtained by inflating the inner envelope (as defined above) by 1.5 times the height of the 50% central region. Any surface crossing the fences are flagged as potential outliers. The factor 1.5 can be also adjusted as in the adjusted functional boxplots to take into account spatial autocorrelation and possible correlations between surfaces.

241 **2.6 Testing for Differences in Median Between Families of Curves or Surfaces**

242 To compare the median curves from two populations of curves, López-Pintado and Romo [2009] proposed  
 243 the rank sum test. Let  $\tilde{\mu}_Y$  and  $\tilde{\mu}_{Y'}$  be the median curves of two populations  $Y$  and  $Y'$  respectively. Define  
 244 the null hypothesis to be

$$H_0 : \tilde{\mu}_Y = \tilde{\mu}_{Y'} \text{ for all } \mu.$$

245 Suppose that we observe two sets of curves, namely  $\{y_1, \dots, y_n\}$  and  $\{y'_1, \dots, y'_m\}$ . Then define the  
 246 reference sample to be  $\{r_1, \dots, r_k\}$  which is from one of the two observed sets with  $k \geq \max(n, m)$ . The  
 247 position of a particular  $y_i$  for  $i = 1, \dots, n$ , or  $y'_j$  for  $j = 1, \dots, m$  with respect to the reference sample  $r$ ,  
 248 is defined as

$$R(y_i) = \frac{1}{n} \sum_{l=1}^n \mathcal{I}\{MBD(z_l) \leq MBD(y_i)\},$$

$$R(y'_j) = \frac{1}{m} \sum_{l=1}^m \mathcal{I}\{MBD(z_l) \leq MBD(y'_j)\},$$

250 where  $MBD$  is the modified band depth defined in previous section, and  $\mathcal{I}$  is the indicator. Then we  
 251 can order the values  $R(y_i)$  and  $R(y'_j)$  from the smallest to the largest, and their ranks are between 1 and  
 252  $n + m$ . The test statistics  $T = \sum_{l=1}^m \text{rank } R(y'_j)$ , then under the null hypothesis  $H_0$ , the distribution of  
 253  $T$  is the distribution of the sum of  $m$  numbers that are randomly chosen from  $1, 2, \dots, n + m$  (Sun and  
 254 Genton [2012b]).

255 **2.7 Remarks on the applications of functional and surface boxplots**

256 In this paper, we use functional and surface boxplots to explore the structure of EEGs. However, these  
 257 methods are general and can be applied to other types of data such as growth data and climate time  
 258 series (Sun and Genton [2012b]).

259 **3 Simulation Study**

260 The purpose of the simulation study is to examine the performance of the exploratory spectral methods  
 261 under various experimental settings. In Section 3.1, we demonstrate the performance of the FBP on the  
 262 smoothed log periodograms of a mixture of two first order autoregressive time series, denoted AR(1). In  
 263 Section 3.2, we illustrate the rank sum test to compare the functional median from two families of curves.

264 **3.1 Functional Boxplot Simulation Study**

265 For the  $r^{th}$  epoch, let  $U_{1r}(t)$  be an AR(1) process with its spectra dominated by high frequencies and  
 266  $U_{2r}(t)$  be another AR(1) with its spectra mostly containing low frequencies. The AR(1) parameters are  
 267 allowed to vary across epochs. Here, we set  $t \in T = \{1, \dots, 1000\}$ . We define  $X_r(t)$  to be the mixture of  
 268  $U_{1r}(t)$  and  $U_{2r}(t)$ , such that

$$X_r(t) = a_{1r}U_{1r}(t) + a_{2r}U_{2r}(t)$$

269 where  $r = 1, \dots, 220$ ,  $a_{1r}$  and  $a_{2r}$  are weighted coefficients of  $U_{1r}(t)$  and  $U_{2r}(t)$  respectively. Then, the  
 270 model for high and low frequency AR(1) processes are defined as

$$U_{\ell r}(t) = \phi_{\ell r} U_{\ell r}(t-1) + W_{rt}$$

where  $\ell = 1, 2$  and  $W(t)$  is white noise. In this setting, the high and low frequency AR(1) are distinguished

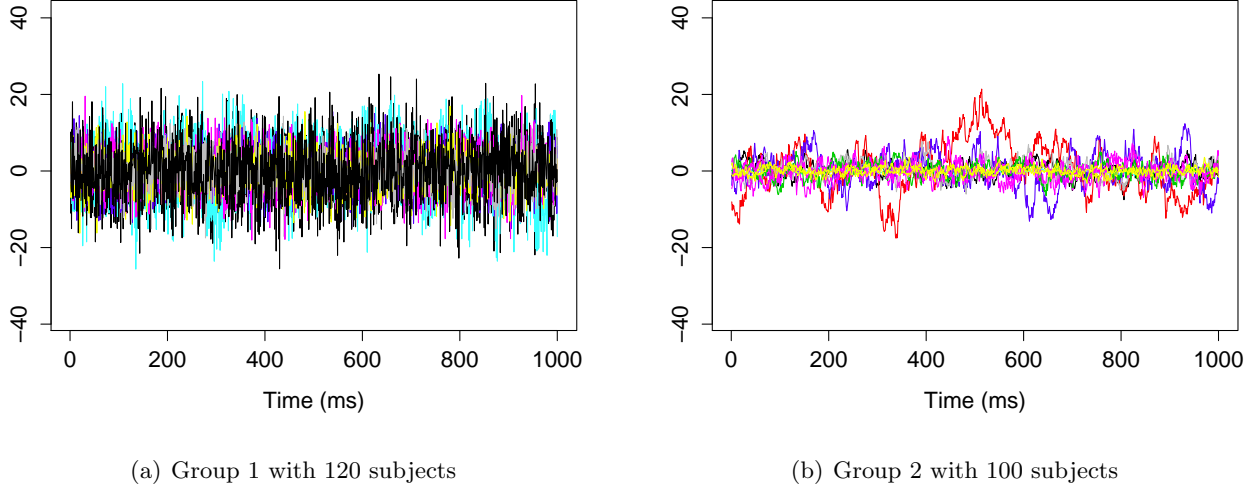


Figure 6: Time series AR(1) for group 1 and group 2

271 by the value of  $\phi_{\ell r}$ . For example, for high frequency  $U_{1r}(t)$ , we set  $\phi_{1r} = 0.9 + \xi_r$ , where  $\xi_r$  are independent  
 272 and identically distributed from  $\mathcal{N}(0, 0.001)$ . Similarly, for low frequency  $U_{2r}(t)$ , we set  $\phi_{2r} = -0.5 + \eta_r$ ,  
 273 and  $\eta_r$  are also independent and identically distributed from  $\mathcal{N}(0, 0.001)$ . Here, we need the variance of  
 274  $\xi_r$  and  $\eta_r$  to be small so that it guarantees causality, i.e.  $\xi_r \in (-1, 1)$  and  $\eta_r \in (-1, 1)$ . Next, we split the  
 275 220 subjects into two groups, such that the first group will include both high and low frequency series,  
 276  $U_{1r}(t)$  and  $U_{2r}(t)$ , while the second group will only have the high frequency series  $U_{1r}(t)$ . To split  $X_r(t)$   
 277 into two groups, we set the weight coefficients  $a_{1r}$  and  $a_{2r}$  as following  
 278

$$a_{1r} \sim \mathcal{N}(10, 1) \text{ for } r = 1, \dots, 220$$

$$a_{2r} \sim \mathcal{N}(5, 1), \text{ for } r = 1, \dots, 120, \text{ and } a_{2r} \sim \mathcal{N}(0, 0.001) \text{ for } r = 121, \dots, 220.$$

280 The two groups of  $X_r(t)$  are shown in Figure 6. Using the gamma generalized crossvalidation method,  
 281 Figure 7 displays the log bias-corrected periodograms for each group, and Figure 8 shows the corresponding  
 282 FBPs. Note that group 1 is dominated by both high (right) and low (left) frequencies while group 2  
 283 includes only low frequencies. Thus, the functional median of group 1 should have two peaks, one each  
 284 in high and low frequency ranges, while the functional median of group 2 has only one peak in the low  
 285 frequency range. In Figure 8, the black curve is the median curve in the center of the functional boxplot.  
 286 The two median curves from each group have clearly summarized the typical power distribution for each  
 287 group. The blue curves in the center form the envelope of the 50% central region. The blue curves outside  
 288 of the 50% central region are the non-outlying minimum and maximum curves. It is worth remarking  
 289 that the envelope of group 1 is smaller than the envelope of group 2, and therefore, we demonstrate that

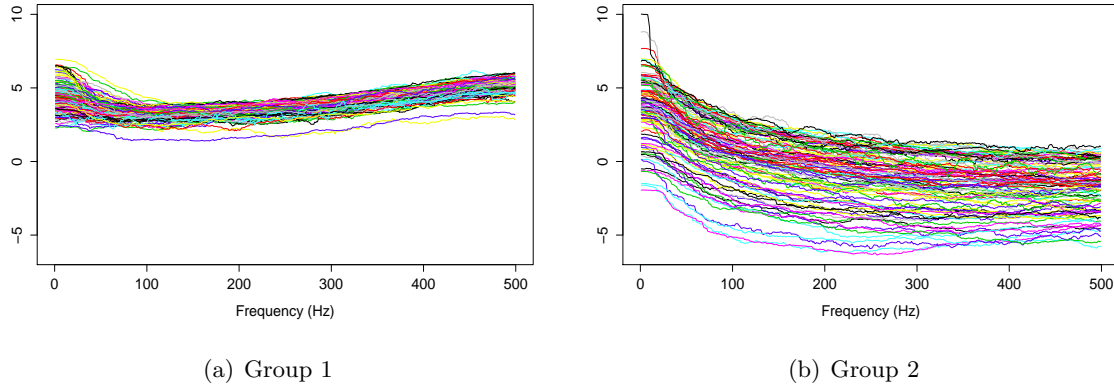


Figure 7: Smoothed log bias-corrected periodograms for Group 1 and Group 2

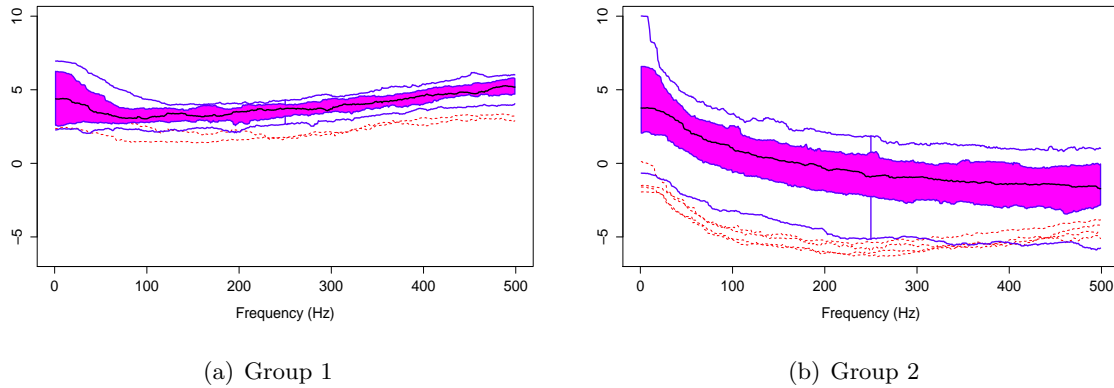


Figure 8: Functional boxplots of Group 1 and Group 2 with a black curve representing the median curve, the pink area denoting the 50% central region, the two inside blue curves indicating the envelopes of 50% central region, the two outside blue curves representing for two non-outlying extreme curves, and the red dashed curves illustrating the outlier candidates detected by 1.5 times the 50% central region rule.

group 2 has more dispersion than group 1. Moreover, the envelope of group 1 is in the middle of the non-outlying minimum and maximum curves, while the envelope of group 2 tends to move upwards. This indicates that group 2 shows more skewness than group 1. The red dashed curve in Figure 8 denotes the outliers. We see that the curves from group 1 that are dominated by high frequencies only are detected as outliers while the curves from group 2 that include both high and low frequencies are detected as outliers.

295

In order to illustrate the usefulness of the functional boxplot compared to the pointwise boxplot, we introduce a simulation study which randomly chooses 10 bias-corrected log periodograms among 160 total periodograms. We simulate an outlying curve by adding additional noise across the 0-100 Hz frequency range, and close to the center for the remaining frequencies. Figure 9-a shows the simulation data including the 10 random bias-corrected log periodograms (grey curves) and a simulated outlying curve (red curve). In Figure 9-b, the functional boxplot successfully detects the simulated outlying curve and other outliers. However, Figure 9-c shows that the pointwise boxplot fails to detect the simulated

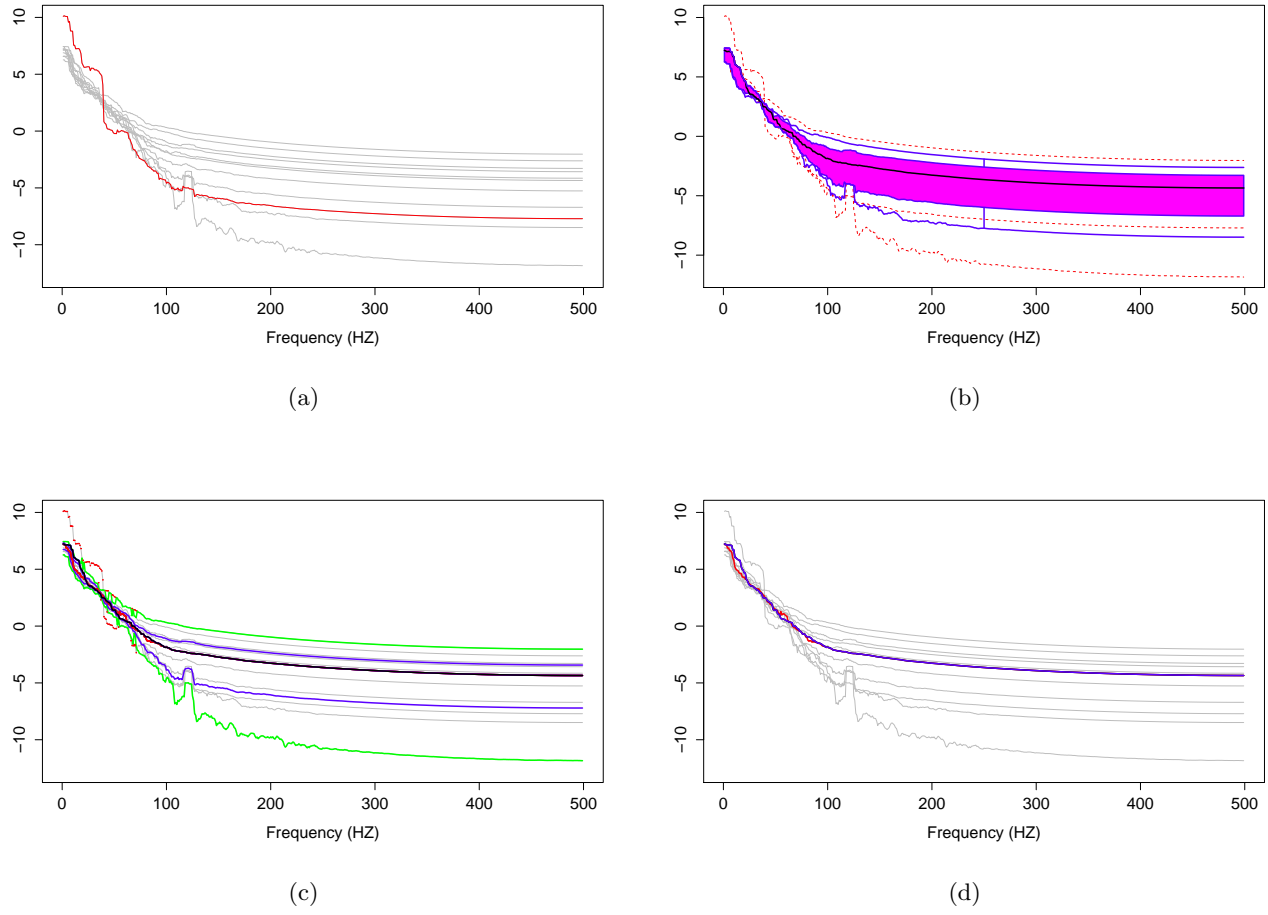


Figure 9: (a) Simulation data with grey curves representing sample curves, a red curve denoting the simulated outlying curve (b) Functional boxplots, (c) Pointwise boxplots with black curve representing a mean curve, blue curves for the envelope of the 50% central region, the green curves for the non-outlying minimum and maximum curves, and the red points for outliers, and (d) two median curves obtaining by functional boxplots method (blue) and pointwise boxplot method (red) are shown in the same plot.

303 outlying curve, and provides some disconnected outlying curves across frequencies. We also notice that  
 304 the non-outlying maximum and minimum curves of pointwise boxplot are actually the outlying curves  
 305 detected by functional boxplot. Figure 9-d compares the two median curves from these two methods,  
 306 and by visual inspection, there is a slight difference between the two median curves at low frequencies.  
 307 Thus, functional boxplot can be a non-parametric method to obtain the median curve and the variability  
 308 around it for EEG data compared to pointwise boxplot.

309

### 310 3.2 Rank Sum Test Simulation Study

311 To investigate the performance of this nonparametric test, we simulated two sets of curves, which are  
 312 defined as below:

$$Y_{\ell,r}(\omega_k) = f_\ell(\omega_k) + a_r g(\omega_k) + h_r(\omega_k),$$

313 where  $r = 50$ ,  $\ell = 1, 2$ ,  $g(\omega_k) = 1$  for all  $\omega_k$ , and  $\omega_k$  is defined as  $\omega_k = k/100$ , where  $k = 1, \dots, 100$ . In  
 314 the model,  $f_1(\omega_k)$  and  $f_2(\omega_k)$  are the mean functions;  $a_r \stackrel{\text{iid}}{\sim} N(0, 5)$  and  $h_r(\omega_k) \stackrel{\text{iid}}{\sim} N(0, 2)$  represent the  
 315 variation between and within the curves, respectively. Let the function  $f_1(\omega_k)$  be defined as

$$f_1(\omega_k) = 5 \cdot \sqrt{1000 \cdot \omega_k},$$

316 and consider three different cases:

- 317 1. The two means are identical, let  $f_2(\omega_k) = f_1(\omega_k)$  for all  $\omega_k$ .
- 318 2. There is a slight deviation between the two means; define  $f_2(\omega_k) = 5 \cdot \sqrt{900 \cdot \omega_k}$ .
- 319 3. There is an appreciable deviation between the two means; let  $f_2(\omega_k) = f_1(\omega_k) + 2k/3$ .

320 We applied the kernel average smoother with window size 7 to smooth each curve from these two families.  
 321 Figure 10 illustrates the simulated curves (left panel) and the smoothed curves (right panel). In order to  
 322 investigate the rank sum test performance in each case, we simulated two families of curves and obtain  
 323 p-values of rank sum test; this procedure was repeated 1000 times. Let the type I error  $\alpha$  be 5%, we  
 324 report the percentage of time that the rank sum test rejects  $H_o : f_1(\omega_k) = f_2(\omega_k)$  for all  $\omega_k$  in Table 1.  
 Overall, the rank sum test method performed well in each case. When the two families are identical, this

	First case	Second case	Third case
Percentage of time rejecting $H_o$	44	605	1000

Table 1: Rank Sum test study result.

325  
 326 method rejected the null hypothesis of equality only 44 times (4.4%) out of 1000 times, which is close  
 327 to the nominal  $\alpha$ . When the two families are nearly identical, this method rejects 605 times (the power  
 328 is 60.5%), and when the two families are completely different, the power is 100%. Thus this method  
 329 demonstrates power and sensitivity to differences.

## 330 4 Analysis of Resting-State EEGs Data

### 331 4.1 Data Description

332 In this paper, we analyze EEG data from one participant in a resting-state EEG study approved by the  
 333 Institutional Review Board of the University of California, Irvine. The over-arching aim of this study was  
 334 to identify a pattern of EEG-derived coherence acquired during rest-state that could predict subsequent  
 335 response to training on a novel motor skill. During EEG acquisition, subjects sat quietly with both feet  
 336 flat on the floor, and were instructed to fixate their gaze to the center of a fixation cross. Each recording  
 337 was 3 minutes in duration. While the original EEG recording included 256 channels, only 194 were used in  
 338 subsequent analyses, as extra-brain artifacts, including cheek and neck muscle artifacts and heart rhythms,  
 339 are more likely to contaminate EEG signals recorded from electrodes overlying cheek and neck regions.  
 340 Following data acquisition, pre-processing steps included: 100 Hz low pass filter; EEG segmentation  
 341 into 1-second consecutive, non-overlapping epochs; mean detrend; and EEG signal re-reference to mean

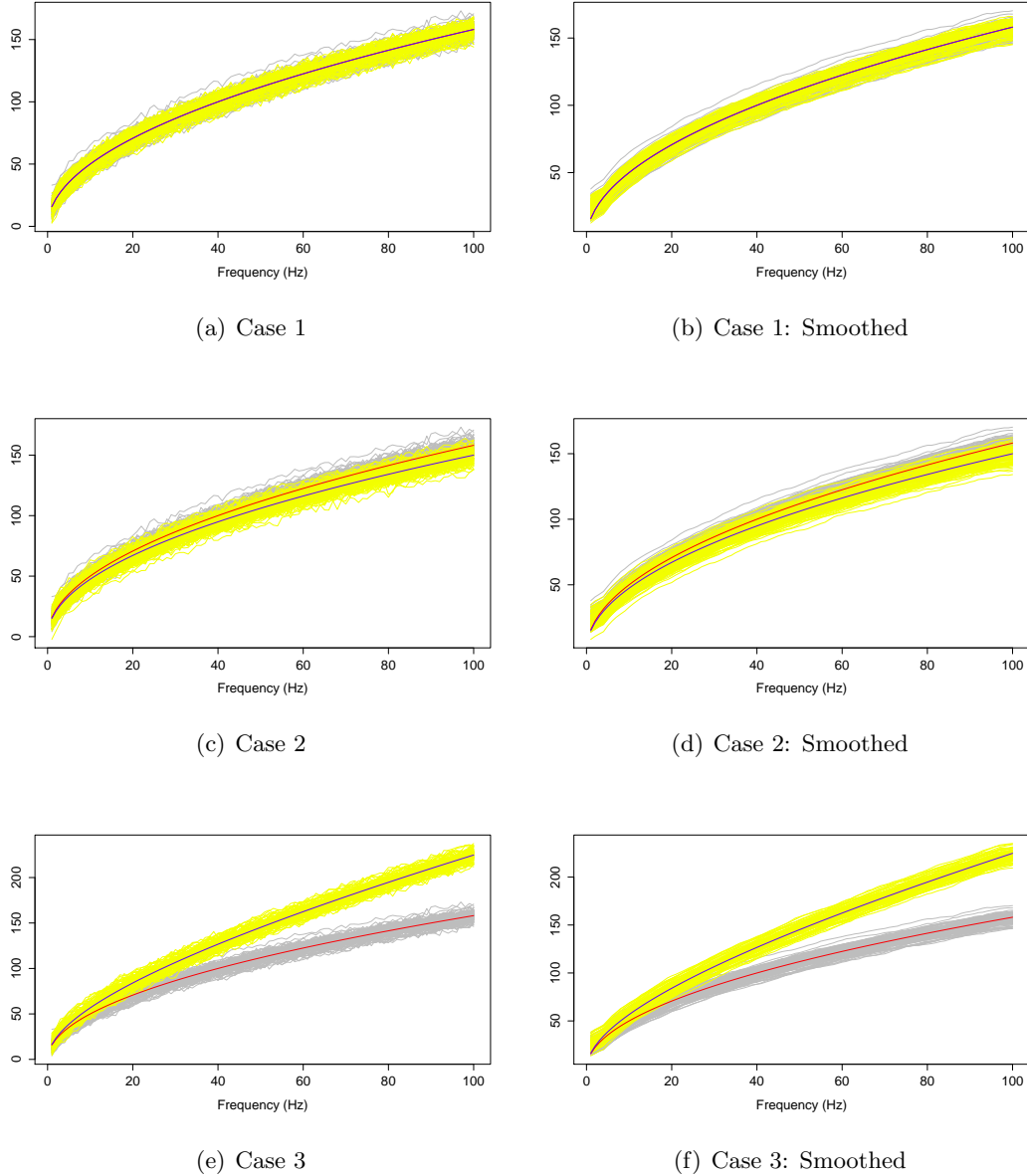


Figure 10: The two families of simulated curves,  $Y_{1,r}$  and  $Y_{2,r}$ . The grey shaded area represents the first family, and the yellow shaded area is for the second family. The red and blue lines are the first and second mean functions,  $f_1$  and  $f_2$ , respectively.

signal across all 194 channels. In addition, a combination of visual inspection and Infomax Independent Component Analysis decomposition were used to remove extra-brain artifacts, including eye blinks, eye movements, muscle artifact, and heart rhythm artifacts. The final dataset consisted of 160 epochs, with each epoch lasting 1 second, and  $T = 1000$  time points for each epoch.

The goals of the present analysis are as follows: In Section 4.2, we closely examined a representative channel in the pre-motor region (specifically channel 197 in this dataset). Since EEGs are not well localized in space (as opposed to local field potentials), conclusions are constrained to the sensor space. However, electrical activity captured in channel 197 reflects activity roughly around the pre-motor area.

350 Specifically, we estimated the (log) spectrum for each epoch to identify any frequency bin or frequency  
 351 band that accounts for the majority of the power spectrum. Moreover, using the method of estimating  
 352 the functional medians, we obtained an estimate of the median curve from the log periodogram curves  
 353 obtained from several epochs. The median curve is interpreted as a “typical” (log) spectral profile across  
 354 several epochs. Using this method, we also identified outlier curves which could also be interpreted as  
 355 epochs with “unusual” EEG activity. In Section 4.3, we investigated the possibility of non-stationarity  
 356 across the 3 minute resting-state EEG recording. Our specific goal was to compare the log spectrum  
 357 during the early phase (first 60 epochs) of the recording with the log spectrum during the late phase (last  
 358 60 epochs) of the recording, and identify frequency bands that exhibit any differences between the early  
 359 vs late phases. In Section 4.4, we studied the spatial variation of power, at each of the five frequency  
 360 bands: delta, theta, alpha, beta and gamma, across all 194 channels, with the goal of identifying regions  
 361 that exhibit relatively greater proportion of spectral power in each of the five frequency bands of interest.  
 362 Finally, we compared the spatial variation for each of the five bands during the early vs late phases of the  
 resting-state EEG recording.

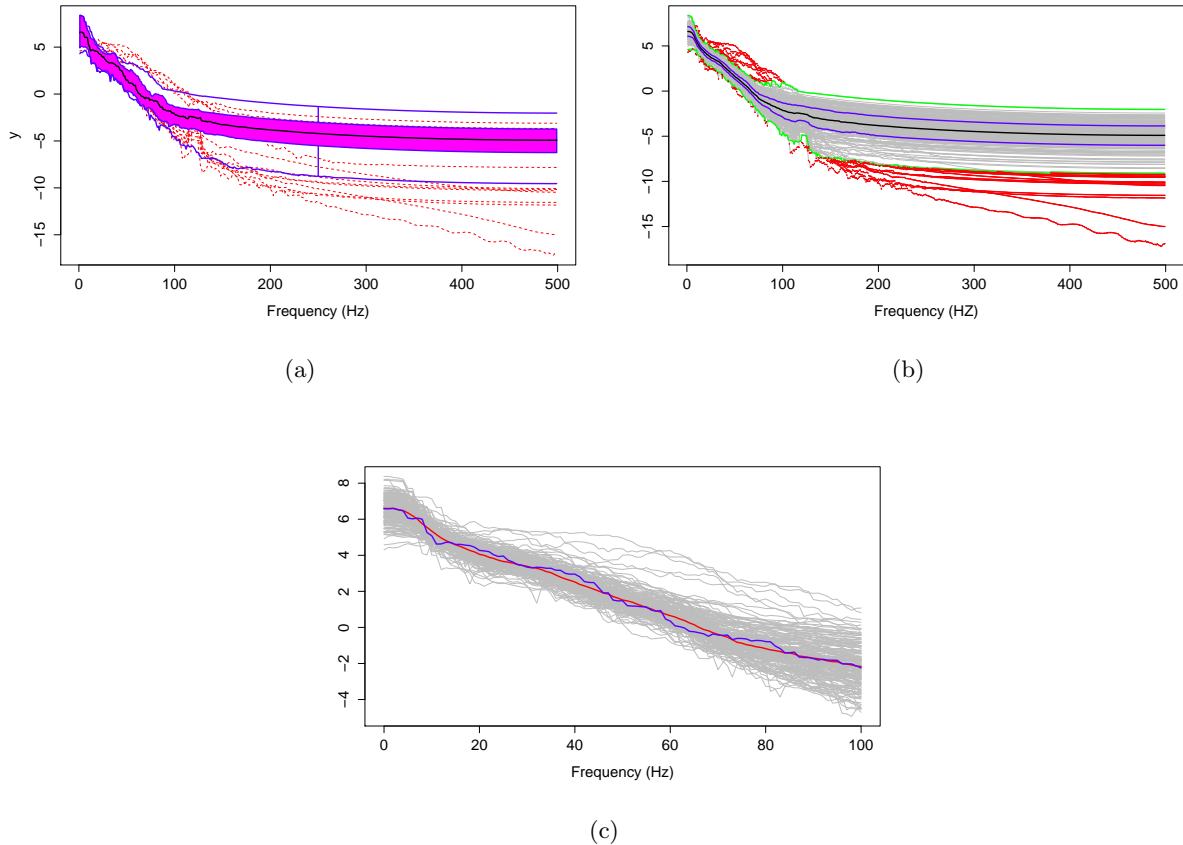


Figure 11: (a) The functional boxplots, (b) Pointwise boxplots of log bias-corrected periodograms, and  
 (c) Two median curves obtaining by functional boxplot method (blue) and pointwise boxplot method  
 (red) are shown in the same plot.

363

364 **4.2 Functional medians of the pre-motor log spectral curves**

365 The log of the bias-corrected periodograms at the representative channel (channel 197) that approximately  
366 overlies cortex of the pre-motor region recorded for several traces and the functional boxplots are displayed  
367 in Figure 11-a. The functional median curve is represented by the black curve, which is located inside  
368 the 50% central region, shaded area. The two blue curves outside of the shaded area are the non-outlying  
369 maximum and minimum curves. Similar to a functional boxplot, we show in Figure 11-b the pointwise  
370 boxplot (per frequency point), where the black curve is the median obtained by connecting the medians at  
371 each frequency point; the blue curves form the central region (50-th percentile region); the green curves are  
372 two non-outlying extreme curves. We compared these two median curves in Figure 11-c and noted a slight  
373 discrepancy between these median curves derived using a functional boxplot and the pointwise boxplot,  
374 with an emphasis on the low frequency range. The main difference between the functional median and the  
375 point-wise median curve is in the interpretation. The former is one of the curves from a recorded epoch,  
376 whereas the latter may not be an actual curve. Hence the latter cannot really be interpreted as a “typical”  
377 curve from a family of curves formed from several epochs. Moreover, the functional boxplots approach  
378 allows us to identify specific epochs that produce “unusual” or outlying log bias-corrected periodogram  
379 curves. Note that in the plots, the grey curves are the log bias-corrected periodograms of 160 epochs and  
380 the red curves are outliers. Figure 11-b also shows that these outlying curves are discontinuous around  
381 the frequency bin centered at 100 Hz.

382 **4.3 Testing for stationarity of EEG epochs across the entire resting-state**

383 In the previous section, the functional boxplot provided descriptive statistics for the log bias-corrected  
384 periodograms of 160 epochs from the pre-motor region. Note that there were originally 180 epochs but 20  
385 had to be removed from further analysis due to extra-brain artifact contamination. Our interest now is  
386 to test whether resting-state brain activity evolved across the 3 minute EEG recording. While there are  
387 many ways to characterize such an “evolution” of the underlying brain processes, here we will specifically  
388 look into changes on the log spectral curves for early vs late phases of the resting-state EEG recording.  
389 In this case, a change in the log spectral power in early vs late phases would indicate non-stationarity of  
390 the EEG signal across the resting-state recording.

391 The null hypothesis of stationarity here is that the true median curves of the early and last phrases  
392 are identical. We test this hypothesis using the rank sum test with the significance level set to 0.05. We  
393 defined the early phase to include the first 60 epochs (60 seconds) of the 3 minute recording and the  
394 late phase to include the last 60 epochs. In Figure 12, we display the functional boxplots and the other  
395 descriptive statistics for each phase. A visual inspection suggests that the median curves are only slightly  
396 different from each other for electrodes that approximately overlie the pre-motor region. More significant  
397 differences are noted for electrodes that approximately overlie the prefrontal region (see Figure 12-c).  
398 Moreover, the rank sum test failed to reject the null hypothesis, as the  $p$ -value is 0.56. Therefore, the  
399 two median curves are not significantly different and the hypothesis of stationarity in the pre-motor  
400 regions is not rejected. This is not entirely unexpected since the whole three-minute recording was purely  
401 resting-state. There was no experimental stimulus and the time frame was short.

402 Next, we use the same testing procedure at this particular channel in the pre-motor region (channel  
403 197) to test the same null hypothesis of non-evolution of the brain process at each of the other channels

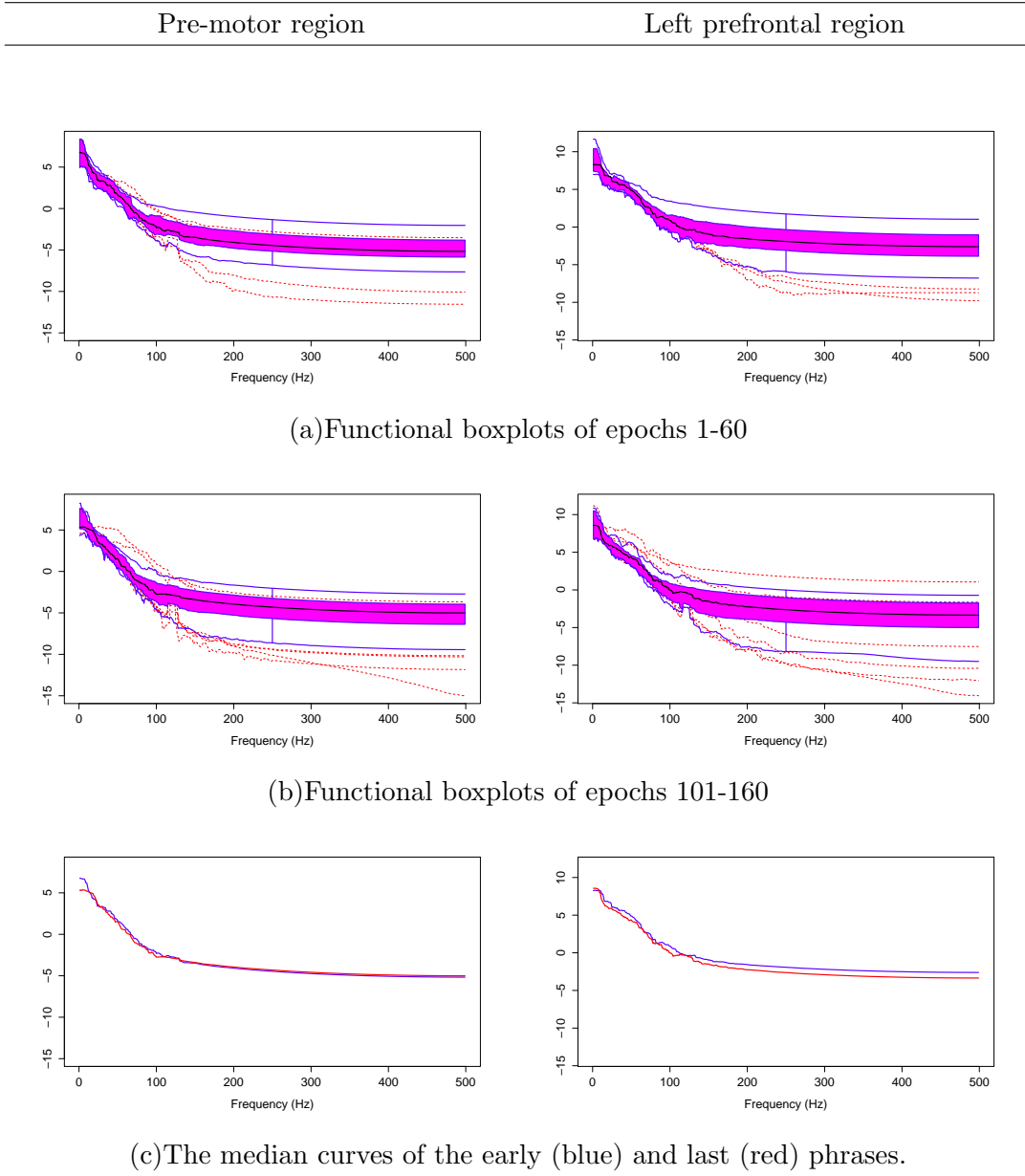


Figure 12: Comparing median curves of the early and last phrases from pre-motor region and left pre-frontal region

across the 3 minute EEG recording. Among the 194 total channels, 18 channels were identified that demonstrated a significant difference in median curves during the early versus late phase at a significance level of 0.05. These channels are represented by colored circles in Figure 13. Of these 18, channel 29 (approximately overlying the supplementary motor area) has the lowest  $p$ -value at  $10^{-4}$ . Since we repeat the same test for 194 channels, we used the Bonferroni correction so that the significance level for each test was set to  $0.05/194 = 2 \times 10^{-4}$ . Indeed, only channel 29 (anterior supplementary motor area) survived the stringent threshold after the Bonferroni correction.

The tests for temporal stationarity at each channel (local spatial tests) revealed several channels having a significant difference between the median curves of the early versus last phases of the EEG recording. As a next step, we studied stationarity in each of 19 predefined regions of the cortex. In this analysis,

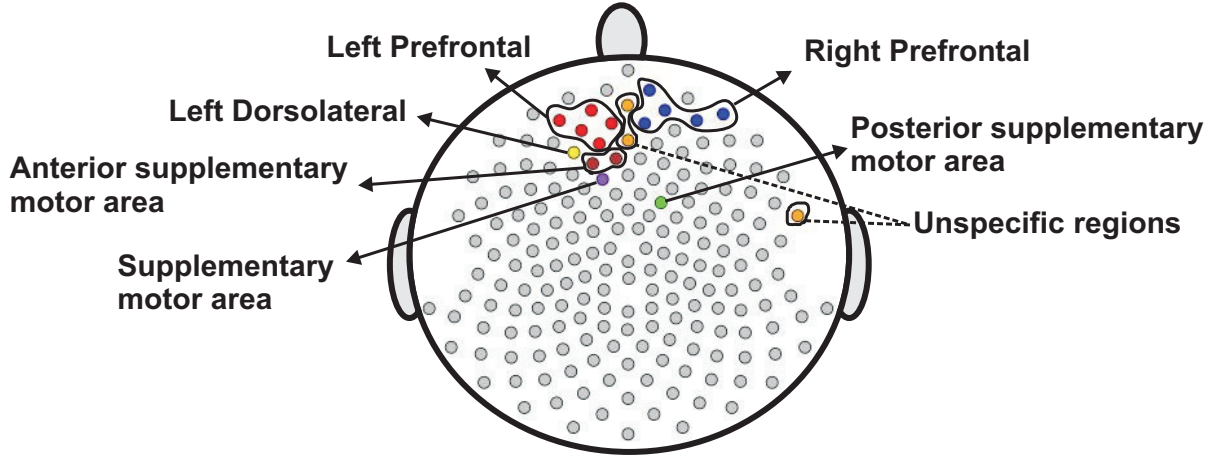


Figure 13: Color circles represent channels, which have significant difference between the median curve of first 60 epochs and the median curve of last 60 epochs at  $\alpha = 0.05$ . Grey circles represent channels which do not have significant difference between the median curve of first 60 epochs and the median curve of last 60 epochs at  $\alpha = 0.05$ .

414 the representative EEG signal for each region was obtained by averaging the EEG signal-epochs over all  
 415 channels within each region. The plots in Figure 14 suggest that the median curves for the early versus  
 416 late phases of the EEG recording are similar for EEG signals recorded from channels that approximately  
 417 overlie right pre-motor and anterior supplementary motor regions, but different in the right pre-frontal  
 418 and left parietal regions. Indeed, we conclude from the rank sum test that there is significant difference  
 419 between the early versus late phases in cluster of channels that approximately overlie the right pre-frontal  
 420 ( $p$ -value = 0.01) and the parietal regions ( $p$ -value = 0.029). We found that the right pre-frontal region  
 421 is significantly non-stationary (i.e., early and late phases differ) at level 0.05 (see Figure 15). This result  
 422 overlaps with the channel-specific tests, in which several of the channels identified to be non-stationary  
 423 in the single channel tests are included in the predefined right pre-frontal region. In contrast, while the  
 424 cluster of electrodes that overlie the left parietal region was found to be non-stationary in the region-by-  
 425 region tests, none of the 18 channels that were identified to be non-stationary in the single channel tests  
 426 are part of the left parietal cluster. Therefore, the additional averaging step across group of channels  
 427 may improve signal-to-noise in this type of analysis. A similar phenomenon was also noted for predefined  
 428 clusters of electrodes overlying at the left pre-frontal region.

#### 429 4.4 The variation of spectral power at each frequency band across the entire cortex

430 Our goal here is to test whether the spectral power at each frequency band differed across the cortical  
 431 surface. We first computed the estimate of the spectral power for each channel at each epoch. Starting  
 432 with the delta band, for each epoch we construct a 2 –  $D$  surface plot of the delta power across the entire  
 433 cortical surface of 194 channels. These surfaces were then grouped according to the early and late phases

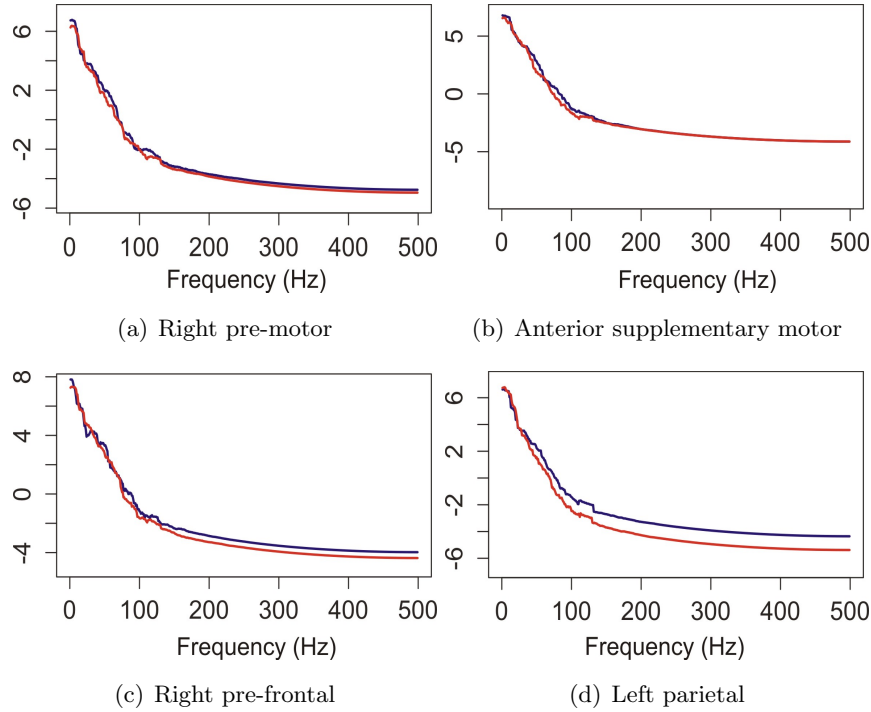


Figure 14: Median curves of the early phase (first 60 epochs, in blue) and the late phase (last 60 epochs, in red) in the right pre-motor, anterior supplementary motor, right pre-frontal and left parietal regions

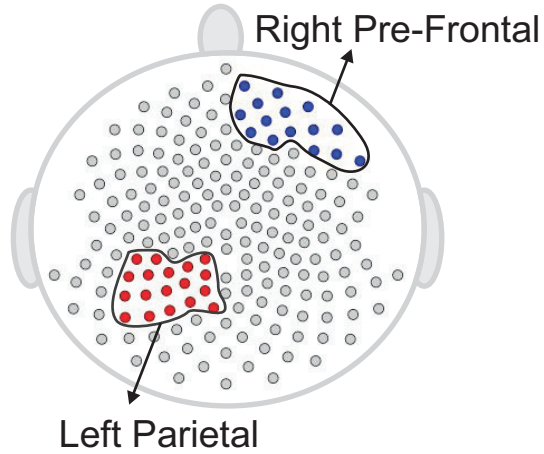


Figure 15: Testing for difference between the early and late phases of the resting-state for each region. The right pre-frontal regions (blue circles) and the left parietal regions (red circles) exhibit significant non-stationarity at level 0.05.

434 of the resting-state. We then applied the surface boxplot method for each frequency band to obtain the  
 435 median surfaces. In Figure 16, we present the median surface for five frequency bands in the early and  
 436 late phases. The color blue represents the low spectral power while red is for high power. In Figure 16, it  
 437 is interesting that even during resting-state there is relatively high spectral power at the beta and gamma

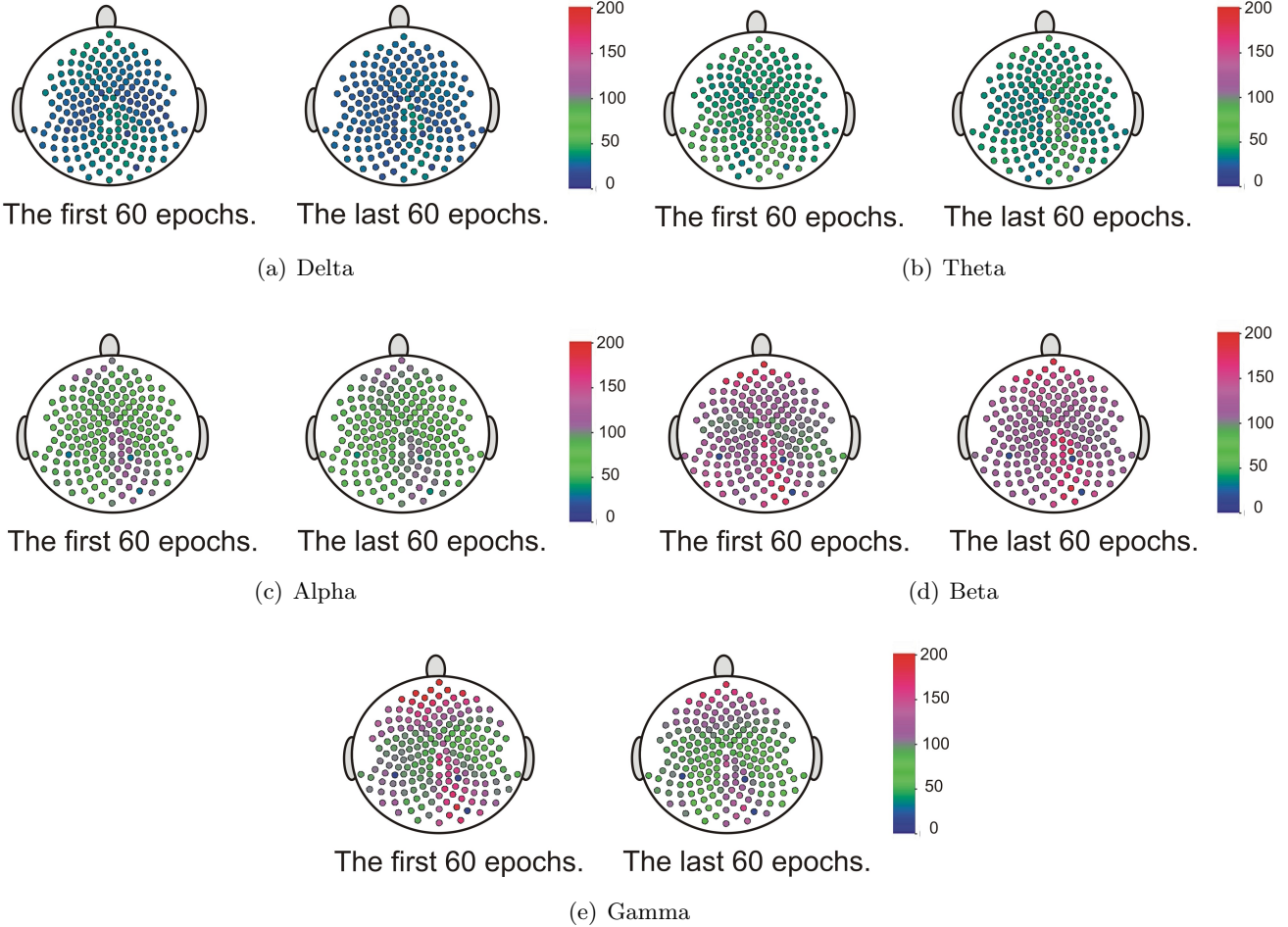


Figure 16: The median surfaces of five frequency bands.

bands – which are both associated with higher cognitive processing (Engel and Fries [2010]).

The next step is to test for differences between the early and late phases of the EEG recording for each of the five frequency bands of interest. Using the rank sum test, the delta and alpha bands do not have significant difference between the early and late phases. However, theta, beta and gamma bands show significant differences. In Figure 17, the colored regions indicate significant differences between the first and last phases while the grey color regions indicate no significant differences between these two phases. For the theta band, the rank sum test rejected the null hypothesis at only one region which is the cluster of electrodes overlying anterior supplementary motor. For the beta band, the rank sum test identified differences at the left medial parietal region. For the gamma band, there were 13 regions (out of 19) with significant difference between the early and late phases. Since the gamma band is wider than other bands, an estimated spectrum powers' variation across channel in gamma band is expected to be smaller than the estimated spectrum powers' variation in other bands. In Section 4.3, we tested the stationarity for each region. Figure 15 shows two regions, namely, the right pre-frontal and left parietal, which are significantly non-stationary across all frequencies between the early and late phases. Figure 17 shows that the cluster of electrodes overlying the left parietal region exhibits significant non-stationarity in the beta and gamma bands while the cluster of electrodes overlying the right pre-frontal region is significantly

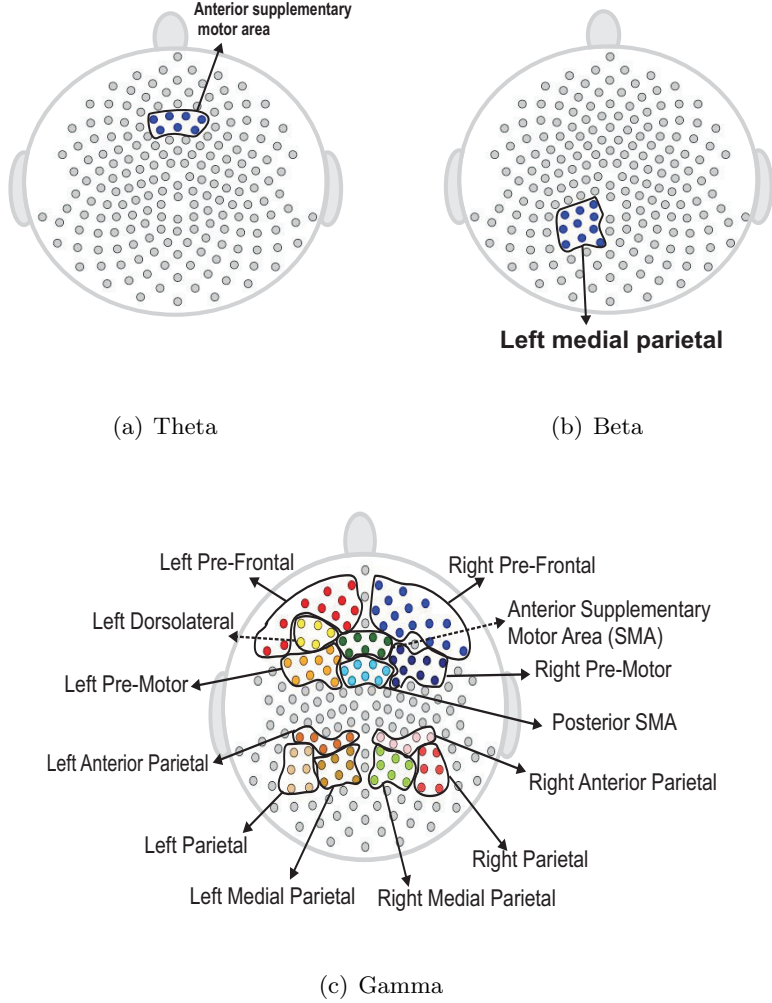


Figure 17: Rank sum test results for regions. Color circles in a bounded curve represents a region, which has a significant difference between the first 60 epochs and the last 60 epochs.

454 non-stationary only in the gamma band.

## 455 5 Conclusion

456 This study has extended the use of the classical boxplot to FBP, which is a new visualization tool to analyze  
 457 functional neuroimaging data, including EEG. The primary findings from the current study demonstrate  
 458 the functional boxplot is useful for both characterizing the spectral distribution of both simulated and  
 459 real EEG data and identifying potential outliers in a continuous EEG signal.

460 In the current implementation of the FBP, ranked sample curves are used to characterize the EEG  
 461 spectrum by defining a 50% central region, a median curve, and maximum and minimum non-outlying  
 462 curves. Thus, the shape, size, and length of the functional boxplot can be used to characterize the distri-  
 463 bution of the dataset, including the skewedness and degree of variability of the EEG recording. Therefore,  
 464 potential application of the FBP in this context includes comparing functional boxplots derived from EEG  
 465 recordings before and after an experimental intervention (e.g., across a period of motor skill training),

466 comparing mean functional boxplots derived from EEG recordings in healthy and diseased experimental  
467 groups, and comparing mean functional boxplots derived from EEG recordings during resting-state versus  
468 task.

469 An additional use of the FBP, as demonstrated by the current results, is to identify potential outliers of  
470 the EEG recording. Extra-brain artifacts, including eye blinks, eye movements, heart rhythms measured  
471 at pulse points downstream, and muscle movements can cause large deviations in the EEG signal, and  
472 represent a significant hurdle in EEG signal processing (Delorme et al. [2007]). As a method for identifying  
473 outliers in the EEG signal, the FBP could be used to rapidly identify periods of an EEG recording  
474 that show high likelihood for contamination by artifacts. In clinical applications, the continuous EEG  
475 recording has demonstrated promise as a method for monitoring neural function in patients who have  
476 compromised level of consciousness (Fyntanidou et al. [2012]) or changes in neural function in patients  
477 undergoing neurosurgical interventions (de Vos et al. [2008]). The use of FBP to identify outliers in the  
478 EEG recording represents a novel method for determining periods of the EEG recording that represent  
479 changes in consciousness in patients with a compromised level of consciousness, or for determining changes  
480 in neural function across neurosurgical intervention.

481 The current study also presents an application of the FBP to examine resting-state EEG data acquired  
482 from a single individual by comparing EEG signals acquired during early versus late phases of the 3 minute  
483 EEG recording. This result has important implications for resting-state studies of neural activity, as many  
484 neuroimaging studies that examine resting-state brain function assume resting-state neural activity to be  
485 static. However, recent studies that examine dynamic changes in resting-state neural activity suggest  
486 momentary change in cognitive processes can cause non-stationarity in resting-state function (Chang  
487 and Glover [2010] and Hansen et al. [2015]). In contrast, the current results show that the majority of  
488 channels demonstrate stationarity across the recording period, and provide support for the assumption  
489 that the average EEG signal is static across a 3 minute EEG recording. Combined with previous findings,  
490 the current results suggest that while momentary changes in cognitive processes result in non-stationary  
491 fluctuations of the time series, when averaged across a 60 second subset of the complete 3 minute EEG  
492 recording, the EEG signal is relatively static. This is supported by the current results that show channels  
493 which demonstrate non-stationarity of the EEG signal when comparing early and late phases of the  
494 recording include electrodes that overlie the right prefrontal region, which is associated with higher-  
495 order cognitive processes (Logue and Gould [2014]). Thus, the assumption of stationarity in resting-state  
496 functional neuroimaging studies may be more appropriate for non-cognitive networks, including the motor  
497 network. Regardless, further work is needed to determine the minimal time-frame in which EEG signal  
498 demonstrate stationarity.

499 Additional future work is focused on developing a new method for computing confidence bands for the  
500 median curve. This method needs to consider the data as a whole. One possible approach is a re-sampling  
501 method, in which the notion of band depth is used to construct a 95% confidence band. A potential  
502 limitation of the re-sampling method is that there is the potential for multiple curves demonstrating ties  
503 with respect to band depth, thus affecting the resultant confidence band. One of the assumptions of the  
504 current smoothed periodogram method is that the log bias-corrected periodogram is an unbiased estimator  
505 of spectrum. Future work will provide further investigation of this assumption as the current method  
506 includes several levels of periodogram manipulation, including smoothing with the gamma generalized  
507 crossvalidation, log transformation, and correction by adding Euler Mascheroni constant. In conclusion,

508 the current study presents a novel implementation of the functional boxplot and demonstrates promise as  
509 a method for exploratory analysis of complex, high-dimensional neuroimaging datasets, including EEG  
510 data.

511 **References**

- 512 T Bohlin. Comparison of two methods of modeling stationary eeg signals. *IBM Journal of Research and*  
513 *Development*, 17(3):194–205, 1973.
- 514 Steven L Bressler and Walter J Freeman. Frequency analysis of olfactory system eeg in cat, rabbit, and  
515 rat. *Electroencephalography and clinical neurophysiology*, 50(1):19–24, 1980.
- 516 David R Brillinger. *Time series: data analysis and theory*, volume 36. SIAM, 1981.
- 517 Peter J Brockwell and Richard A Davis. *Time series: theory and methods*. Springer Science & Business  
518 Media, 2009.
- 519 Catie Chang and Gary H Glover. Time-frequency dynamics of resting-state brain connectivity measured  
520 with fmri. *Neuroimage*, 50(1):81–98, 2010.
- 521 Cecile C de Vos, Susan M van Maarseveen, Paul JAM Brouwers, and Michel JAM van Putten. Continuous  
522 eeg monitoring during thrombolysis in acute hemispheric stroke patients using the brain symmetry  
523 index. *Journal of Clinical Neurophysiology*, 25(2):77–82, 2008.
- 524 Arnaud Delorme, Terrence Sejnowski, and Scott Makeig. Enhanced detection of artifacts in eeg data  
525 using higher-order statistics and independent component analysis. *Neuroimage*, 34(4):1443–1449, 2007.
- 526 Andreas K Engel and Pascal Fries. Beta-band oscillations-signalling the status quo? *Current opinion in*  
527 *neurobiology*, 20(2):156–165, 2010.
- 528 Jianqing Fan and Eva Kreutzberger. Automatic local smoothing for spectral density estimation. *Scandi-*  
529 *navian Journal of Statistics*, 25(2):359–369, 1998.
- 530 Mark Fiecas and Hernando Ombao. Modeling the evolution of dynamic brain process during a learning  
531 association experiment. *Journal of the American Statistical Association*, (Under revision), 2015.
- 532 B Fyntanidou, V Grosomanidis, Z Aidoni, G Thoma, M Giakoumis, E Kiurzieva, and C Skourtis. Bis-  
533pectral index scale variations in patients diagnosed with brain death. In *Transplantation proceedings*,  
534 volume 44, pages 2702–2705. Elsevier, 2012.
- 535 Hong-Ye Gao. Choice of thresholds for wavelet shrinkage estimate of the spectrum. *Journal of Time*  
536 *Series Analysis*, 18(3):231–251, 1997.
- 537 Marc G Genton, Christopher Johnson, Kristin Potter, Georgiy Stenchikov, and Ying Sun. Surface box-  
538 plots. *Stat*, 3(1):1–11, 2014.
- 539 Enrique CA Hansen, Demian Battaglia, Andreas Spiegler, Gustavo Deco, and Viktor K Jirsa. Functional  
540 connectivity dynamics: Modeling the switching behavior of the resting state. *NeuroImage*, 105:525–535,  
541 2015.
- 542 Anders Isaksson, Arne Wennberg, and Lars H Zetterberg. Computer analysis of eeg signals with para-  
543 metric models. *Proceedings of the IEEE*, 69(4):451–461, 1981.

- 544 Shikha Jain and Gopikrishna Deshpande. Parametric modeling of brain signals. In *Biotechnology and*  
545 *Bioinformatics, 2004. Proceedings. Technology for Life: North Carolina Symposium on*, pages 85–91.  
546 IEEE, 2004.
- 547 Raed A Joudi, Ned Jenkinson, John-Stuart Brittain, Tipu Z Aziz, and Peter Brown. Driving oscillatory  
548 activity in the human cortex enhances motor performance. *Current Biology*, 22(5):403–407, 2012.
- 549 Andrew D Krystal, Raquel Prado, and Mike West. New methods of time series analysis of non-stationary  
550 eeg data: eigenstructure decompositions of time varying autoregressions. *Clinical Neurophysiology*, 110  
551 (12):2197–2206, 1999.
- 552 Thomas CM Lee. A simple span selector for periodogram smoothing. *Biometrika*, 84(4):965–969, 1997.
- 553 Sheree F Logue and Thomas J Gould. The neural and genetic basis of executive function: attention,  
554 cognitive flexibility, and response inhibition. *Pharmacology Biochemistry and Behavior*, 123:45–54,  
555 2014.
- 556 Sara López-Pintado and Juan Romo. On the concept of depth for functional data. *Journal of the American*  
557 *Statistical Association*, 104(486):718–734, 2009.
- 558 Scott Makeig. Auditory event-related dynamics of the eeg spectrum and effects of exposure to tones.  
559 *Electroencephalography and clinical neurophysiology*, 86(4):283–293, 1993.
- 560 Scott Makeig, Anthony J Bell, Tzyy-Ping Jung, Terrence J Sejnowski, et al. Independent component  
561 analysis of electroencephalographic data. *Advances in neural information processing systems*, pages  
562 145–151, 1996.
- 563 Peter McCullagh and John A Nelder. Generalized linear models. pages 33–4, 1989.
- 564 Paul L Nunez and Ramesh Srinivasan. *Electric fields of the brain: the neurophysics of EEG*. Oxford  
565 university press, 2006.
- 566 Hernando C Ombao, Jonathan A Raz, Robert L Strawderman, and Rainer Von Sachs. A simple generalised  
567 crossvalidation method of span selection for periodogram smoothing. *Biometrika*, 88(4):1186–1192,  
568 2001.
- 569 Yudi Pawitan and Finbarr O’sullivan. Nonparametric spectral density estimation using penalized whittle  
570 likelihood. *Journal of the American Statistical Association*, 89(426):600–610, 1994.
- 571 Donald B Percival and Andrew T Walden. *Spectral analysis for physical applications*. Cambridge University  
572 Press, 1993.
- 573 G Pfurtscheller and A Aranibar. Evaluation of event-related desynchronization (erd) preceding and  
574 following voluntary self-paced movement. *Electroencephalography and clinical neurophysiology*, 46(2):  
575 138–146, 1979.
- 576 Maurice Bertram Priestley. Spectral analysis and time series. 1981.

- 577 Anita K Roopun, Steven J Middleton, Mark O Cunningham, Fiona EN LeBeau, Andrea Bibbig, Miles A  
578 Whittington, and Roger D Traub. A beta2-frequency (20–30 hz) oscillation in nonsynaptic networks of  
579 somatosensory cortex. *Proceedings of the National Academy of Sciences*, 103(42):15646–15650, 2006.
- 580 David S Shumway and David S Stoffer. *Time series analysis and its applications*, volume 3. Springer  
581 New York, 2000.
- 582 R. Srinivasan and S. Deng. Multivariate spectral analysis of eeg: Power, coherence and second-order blind  
583 identification. *The Biomedical Engineering Handbook*, 4, 2011.
- 584 Ying Sun and Marc G Genton. Functional boxplots. *Journal of Computational and Graphical Statistics*,  
585 20(2), 2011.
- 586 Ying Sun and Marc G Genton. Adjusted functional boxplots for spatio-temporal data visualization and  
587 outlier detection. *Environmetrics*, 23(1):54–64, 2012a.
- 588 Ying Sun and Marc G Genton. Functional median polish. *Journal of agricultural, biological, and envi-  
589 ronmental statistics*, 17(3):354–376, 2012b.
- 590 Ying Sun, Marc G Genton, and Douglas W Nychka. Exact fast computation of band depth for large  
591 functional datasets: How quickly can one million curves be ranked? *Stat*, 1(1):68–74, 2012.
- 592 Grace Wahba. Automatic smoothing of the log periodogram. *Journal of the American Statistical Asso-  
593 ciation*, 75(369):122–132, 1980.
- 594 Jennifer Wu, Ramesh Srinivasan, Arshdeep Kaur, and Steven C Cramer. Resting-state cortical connec-  
595 tivity predicts motor skill acquisition. *NeuroImage*, 91:84–90, 2014.